



Synthesis and evaluation of the performance of MWCNTs-CoFe₂O₄ magnetic nanocomposite for adsorption of Remazol Brilliant Blue Reactive: kinetics and thermodynamics study

Hedieh Rahbar^a, Seyed Davoud Ashrafi^b, Kamran Taghavi^{a,*}, Jalil Jaafari^{b,*}

^aDepartment of Environmental Health Engineering, School of Health, Guilan University of Medical Sciences, Rasht, Iran, Tel. +98 131 3229599; Fax: +98 131 3234155; email: k.taghavi@gums.ac.ir (K. Taghavi),

Tel. +98 131 3229599; Fax: +98 131 3234155; email: hedieh.rahbar@yahoo.com (H. Rahbar)

^bResearch Center of Health and Environment, School of Health, Guilan University of Medical Sciences, Rasht, Iran,

Tel. +98 131 3229599; Fax: +98 131 3234155; email: jalil.jaafari@gums.ac.ir (J. Jaafari), Tel. +98 131 3229599;

Fax: +98 131 3234155; email: d_ashrafi@yahoo.com (S.D. Ashrafi)

Received 30 October 2021; Accepted 29 July 2022

ABSTRACT

In this research, multi-walled carbon nanotubes-CoFe₂O₄ magnetic (MWCNTs-CoFe₂O₄) based-magnetic nanocomposite was used for removal of Remazol Brilliant Blue Reactive (RBBR) dye, which is one of the most widely used organic dyes in the textile industry. The various characterization methods such as Fourier-transform infrared spectroscopy, field-emission scanning electron microscopy, X-ray diffraction, energy-dispersive X-ray spectroscopy, transmission electron microscopy, Brunauer–Emmett–Teller and vibrating sample magnetometer were used to confirm the formation of nanocomposite adsorbent and study its magnetic properties. The effective parameters on the removal process were time, adsorbent dose, dye concentration, pH and temperature. The optimal values of each of these parameters were determined as 40 min, 0.4 g, 20 mg/L, 3 and 298 K, respectively. The removal efficiency of RBBR dye in the presence of MWCNTs-CoFe₂O₄ nanocomposite was 95% under optimal conditions. The maximum adsorption capacity (q_{max}) of MWCNTs-CoFe₂O₄ for RBBR dye was 106.5 mg/g. The obtained experimental data were then analyzed with different isotherms such as Langmuir, Freundlich and Temkin and the results showed a very good agreement of the data with the Langmuir isotherm ($R^2 = 0.9998$). In addition, two quasi-first-order and quasi-second-order kinetic models studied the kinetic of the adsorption process. It was observed that the process follows the quasi-second-order kinetic. Finally, a thermodynamic study was carried out at four temperatures of 298, 308, 318 and 328 K to calculate the Gibbs free energy (ΔG) changes, enthalpy changes (ΔH) as well as entropy changes (ΔS). The calculated values for the mentioned thermodynamic parameters were -8.93 kJ/mol, -32.38 kJ/mol and 0.078 kJ/mol K, respectively. The results showed that dye adsorption is an exothermic, spontaneous process and is associated to a reduction in system irregularities.

Keywords: Adsorption; Dye removal; Multi-walled carbon nanotubes; Magnetic adsorbent; Remazol Brilliant Blue Reactive; Textile effluents

* Corresponding authors.

1. Introduction

Dyes compounds, which are one of the largest subsets of industrial organic compounds and are produced in large quantities annually [1,2], in addition to the textile industry are also widely used in other industries such as leather, wood, paper, food, pharmaceuticals, cosmetics, printing, rubber and plastics [3–5]. Studies have confirmed that about 10%–20% of the organic dyes used in the textile industry are wasted during the dyeing process. In addition to organic dyes, effluents produced from the textile industry contain very high amounts of suspended solids, chemical oxygen demand and biochemical oxygen demand, acids and alkalis used for pH adjusting, heavy metals, and many other various chemical compounds. If these compounds are discharged into the environment along with the effluent from the process, they can have adverse effects on the human health [4,6,7].

These compounds have a very high stability due to the presence of aromatic rings and have been proven to be carcinogenic, allergenic and mutagenic in nature. These compounds can cause kidney failure and severe damage to the reproductive system, liver, brain and central nervous system if contact with the human body [8–11]. In addition, the turbidity caused by the presence of suspended particles disrupts photosynthesis and the presence of colored residues affects the beauty of the environment. Accordingly, it can be said that the effluents of the textile industry are in the category of the most toxic industrial effluents because of the presence of many chemical pollutants in it; therefore, it is essential to treat textile effluents before releasing into environment [12,13].

There are different methods including physical, chemical, biological and advanced oxidation methods to remove, degrade and separate organic dyes from industrial effluents. Methods such as adsorption and membrane technology in the category of physical methods, coagulation and flocculation in the category of chemical methods, aerobic and anaerobic purification processes related to biological methods, as well as homogeneous and heterogeneous photocatalytic methods are among the methods that can be used for removal of organic dyes from aqueous solutions [14–19].

Among the various methods for the removal of organic dyes, the adsorption method is known as an effective method due to easy operation, low cost, without the production of sludge, harmful and dangerous intermediate compounds and also low required space [20–22]. From this viewpoint, cost-effective adsorbents with very high efficiency based on carbon materials such as carbon nanotubes (CNTs) and their modification have been considered to increase the level and capacity of this class of adsorbents. Numerous studies have shown that CNTs have a higher level and capacity than other carbon materials such as activated carbon (AC) and at the same time have a shorter equilibrium time. Duta et al. demonstrated that the multi-walled carbon nanotubes was able to simultaneously remove anionic and cationic dyes from aqueous solution. Therefore, they showed that carbon nanotubes, as an efficient adsorbent, have good properties for industrial application to remove various organic dyes from effluents.

Magnetic nanomaterials act as efficient adsorbents due to its easy separation under an external magnetic and field high specific surface area have been used as adsorbents for the adsorption of many pollutants from aqueous solutions [23–25]. Among different magnetic nanomaterials, magnetic iron oxide (Fe_3O_4) nanoparticles are widely used as adsorbents of various contaminants [26,27].

In another study, Li et al. [28], compared the adsorption of Remazol Brilliant Blue Reactive (RBBR) and heavy metal cations of copper on carbon nanotubes with different sizes of carboxyl groups and specific surface area in aqueous solutions. Based on their findings, about 291 mg of RBBR and about 49 mg of copper cation per gram of adsorbent were adsorbed. In this study, it was clearly shown that the adsorption rate was directly dependent on the specific surface area of the adsorbent. Arya et al. [29] also examined the removal of RBBR using activated carbon from the leaves of *Thuja orientalis* as an environmentally friendly method in 2020. RBBR removal was investigated in the concentration range of 0.1–6.65 mmol/L. The highest efficiency was obtained at pH = 6 and contact time of 300 min. In this study, it was found that adsorption was well described by the Freundlich model. The adsorption efficiency was obtained 73% after four consecutive.

Easy separation of the adsorbent from the solution for reuse is another aspect of the design of an effective adsorbent. Recently, much attention has been paid to the separation of the adsorbent from the solution after the removal of contaminants by creating a magnetic field. This method is a fast, easy and very efficient method for separation of the adsorbent from heterogeneous suspension systems.

In this research, the synthesis and application of magnetic carbon nanotubes nanocomposites with high surface area and capacity with the aim of easy separation from the solution by a magnetic field is presented. Therefore, multi-walled carbon nanotubes- CoFe_2O_4 (MWCNTs- CoFe_2O_4) nanoparticles based-magnetic composite for surface adsorption of RBBR is considered. To determine the optimal conditions for dye removal, isotherms, kinetics and thermodynamic parameters, the effect of parameters affecting the adsorption process such as adsorbent dose, dye concentration, time, pH and temperature was investigated. It should be noted that RBBR dye is also known as Reactive Blue 19 (RB19).

2. Materials and methods

2.1. Materials

The materials used in this study were cobalt ferrite (CoFe_2O_4) nanoparticles which prepared by co-precipitation method, iron(III) chloride hexahydrate ($\text{FeCl}_3 \cdot 6\text{H}_2\text{O}$), cobalt(II) chloride ($\text{CoCl}_2 \cdot 6\text{H}_2\text{O}$) and sodium hydroxide (NaOH) as the precipitating agent. These materials were purified and purchased from Merck (Germany). Also for the preparation of multi-walled carbon nanotubes- CoFe_2O_4 nanoparticles based-nanocomposite (MWCNTs- CoFe_2O_4), multi-walled carbon nanotubes with laboratory purity purchased from Merck (Germany) and used for the synthesis of magnetic nanocomposites. Deionized water has also been used as a solvent. In order to adjust pH of the solutions

used in the experiments, 1 M solutions of hydrochloric acid and sodium hydroxide (Merck, Germany) were used. RBBR organic dye as a pollutant was purchased from Alvan Sabet, Iran with commercial purity and used without any secondary purification for preparation of the synthetic effluents in experiments. Some of the physical and chemical properties of dye molecule are shown in Table 1.

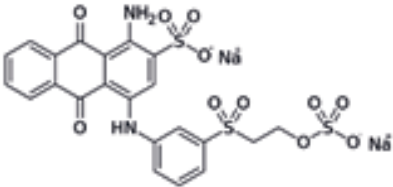
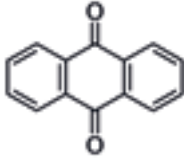
2.2. Synthesis of MWCNTs-CoFe₂O₄ nanocomposite

FeCl₃·6H₂O and CoCl₂·6H₂O were each dissolved separately in 100 mL of deionized water at a molar ratio of 2 to 1. Each solution was then stirred separately for 30 min by a magnetic stirrer. After this step, both solutions were added to each other in a 500 mL beaker and mixed together by stirring. Then, 250 mL of 1 M NaOH solution was prepared separately and added dropwise to the mixture containing FeCl₃·6H₂O and CoCl₂·6H₂O under stirring conditions. pH changes were also controlled by a pH meter. The addition of 1 M NaOH solution was continued until the pH of the solution was exactly 12. After completing all the above steps, the cobalt ferrite cores will appear in a test vessel containing FeCl₃·6H₂O and CoCl₂·6H₂O, and the nucleation phase will begin. Then, in order to start the synthesis of magnetic nanocomposite, a mixture containing of multi-walled carbon nanotubes and ethylene glycol was added to the solution and the mixture was stirred by magnetic stirrer with the high speed (150 rpm). The solution was stirred for 120 min at a constant temperature of 80°C to ensure the completion of the chemical reaction. The nanoparticle growth step begins after the completion of the nucleation stage. To remove impurities as well as disturbing ions in the solution, the obtained precipitate was washed several times with deionized water and then the formed precipitate was separated from the solution by centrifugation. After centrifugation and separation of the solid and liquid phases, the residual nanoparticles were washed several times with deionized water. Finally, the prepared precipitate was placed in an oven for 24 h at 70°C [30,31]. The resulting powder was considered as MWCNTs-CoFe₂O₄ nanocomposite and subjected to various instrumental analyzes for identification and confirmation.

2.3. Characterization of MWCNTs-CoFe₂O₄ nanocomposite

In this study, various characterization methods have been used for identification and analysis of the synthesized nanocomposite. Different techniques such as Fourier-transform infrared spectroscopy (FTIR) analysis, Thermo Company, Model AVATAR, (USA). Field-emission scanning electron microscopy (FESEM), TESCAN Company, Model MIRA 3, (Czech Republic). Energy-dispersive X-ray spectroscopy (EDS), TESCAN Company, Model MIRA 2, (Czech Republic). X-ray diffraction (XRD), PHILIPS Company, Model PW1730, (Netherlands). Transmission electron microscopy (TEM), Model CM120, (Netherlands). Brunauer–Emmett–Teller (BET), BEL Company Model BELSORP MINI II, (Japan) and vibrating sample magnetometer (VSM), Model LBKFB, (Iran) were applied for identification of the functional groups in the adsorbent structure, study the surface characteristics and elemental analysis of the composition, calculation of the size

Table 1
Some physical and chemical properties of RBBR dye

Chemical structure of the dye	
Chromophore (Anthraquinone)	
Molecular formula	C ₂₂ H ₁₆ N ₂ Na ₂ O ₁₁ S ₃
Molecular weight	626.55 g/mol
Maximum wavelength (max.)	590 nm
Degree of purity	Commercial
Nature	Anionic

of crystal particles in the sample, morphology of the nanocomposite structure, calculation of the specific surface area and also study the magnetic properties of the synthesized nanocomposite, respectively.

2.4. Preparation of synthetic effluent and study of dye removal by adsorption method

At the first, a stock solution with a concentration of 1,000 mg/L was prepared from RBBR dye. To perform various experiments and optimization process, a synthetic effluent was prepared in the required volume and concentration by diluting the stock solution. In order to draw the calibration curve (absorption vs. concentration (mol/L)), volumes of 50 mL of dye solutions with different concentrations of 10, 20, 30, 50, 100 and 200 mg/L were prepared for absorption measurements by a UV-Vis spectrophotometer (Model of Cecil CE2021). Based on the Beer–Lambert equation and the calibration curve, the dye molar absorption coefficient was calculated and used for quantification of the unknown concentration of the samples [Eq. (1)]. To investigate the factors affecting the adsorption efficiency such as adsorbent dose, dye concentration, time, pH and temperature, solutions with an initial concentration of 30 mg/L in a volume of 1 L were prepared and the adsorption process was optimized by one factor at a time (OFAT) method. Changes in the concentration of the solution during each of the experiments at regular intervals of the synthetic effluent samples, and then the rate of adsorption of the resulting sample after separation of the adsorbent by a magnet measured it placed. Dye removal efficiency and adsorbent capacity have been calculated based on techniques in accordance with Eqs. (2) and (3). Then, to determine the type of dye adsorption mechanism on the adsorbent, the experimental data were matched with different isotherms under

optimal conditions. Finally, thermodynamic and kinetic parameters of the process were resulted from conducting experiments in which temperature and concentration were considered as effective independent variables.

$$\% \text{Removal} = 1 - \left[\frac{A}{A_0} \right] \times 100 \quad (1)$$

$$q_t = \left(\frac{C_0 - C_t}{m} \right) \times V \quad (2)$$

where A_0 , q_t , C_0 , C_t , m and V are related to the initial absorption of the sample, the adsorbent capacity at time t , the initial solution concentration (mg/L), the sample concentration after t min (mg/L), adsorbent mass (g) and solution volume (L).

3. Results and discussion

3.1. Characterization of adsorbent

3.1.1. FTIR spectroscopy

FTIR spectroscopy as one of the most useful and efficient techniques is used for identification of functional groups of the organic compounds. Fig. 1 shows the FTIR spectrum of the MWCNTs-CoFe₂O₄ nanocomposite in the range of 400–4,000 cm⁻¹. The peaks appeared in the area of 400–600 cm⁻¹, are related to the metal oxide nanoparticles [32]. The sharp peak appeared in the area of 596.71 cm⁻¹ is related to the stretching vibration of the bonds of the metal (Fe, Co) – oxygen (O). The peak formed in the area of 459.51 cm⁻¹ is also related to the stretching vibrations of Co–O bonds. The peaks formed in the areas of 1,383.35 and 1,628.32 cm⁻¹ are related to the asymmetric stretching vibrations of the –COOH and C=C groups of the carbon nanotubes structures, respectively [33]. The band at 2,950 cm⁻¹ assigned to the C–H group of aliphatic section of carbon nanotubes structures. The peaks in around of 3,428.58 cm⁻¹ can be attributed to the symmetric stretching of the O–H groups that is due to ethylene glycol or water molecules adsorbed on the adsorbent surface. The assigned pattern corresponding to this analysis

method can be convincing evidence about the formation of MWCNTs-CoFe₂O₄ nanocomposite [32,33].

3.1.2. FESEM and EDS analysis

To investigate the surface properties, shape and dispersion of the components of the synthetic nanocomposite, FESEM images of MWCNTs-CoFe₂O₄ based-nanocomposite are shown in Fig. 2. In these images, the tubular structures represent multi-walled carbon nanotubes as well as amorphous and sometimes spherical or cubic structures represent cobalt ferrite nanoparticles. The agglomeration phenomenon among cobalt ferrite nanoparticles which can be clearly seen in the 500 nm scale can be led to the formation of dense structures on the adsorbent surface. The agglomeration phenomenon can be attributed to the magnetic interaction and resulted aggregation between CoFe₂O₄ nanoparticles. Also, according to the FESEM image obtained with a resolution of 1 μm, the dispersion of carbon nanotubes and cobalt ferrite nanoparticles among each other is very good. Dispersion between two organic and inorganic parts of the nanocomposite has caused porosity. The diameter of multi-walled carbon nanotubes as well as the size of cobalt ferrite nanoparticles was estimated to be about 90–100 and 50 nm, respectively, and generally the size of all particles was less than 100 nm. Also, to evaluate the chemical composition of synthesized nanocomposite, a nanocomposite sample was analyzed by EDS method. The result of this analysis is shown in Fig. 3. Based on this investigation, it was found that the weight percentages of the constituent elements of this nanocomposite including carbon (C), oxygen (O), iron (Fe) and cobalt (Co), were 71.34%, 17.39%, 7.75% and 3.52%, respectively. Therefore, the detection of Fe and Co elements in the nanocomposite sample by the EDS analysis confirms the formation of the bulk of the MWCNTs-CoFe₂O₄ nanocomposite. Also, based on the obtained information in Table 2, it is determined that predominant part of the nanocomposite consists of carbon nanotubes.

3.1.3. TEM analysis

TEM analysis was used to recognize the morphology of MWCNTs-CoFe₂O₄ nanocomposite with high precision

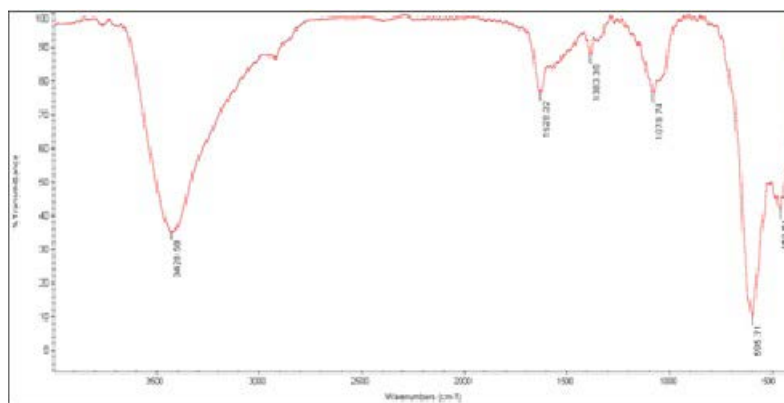


Fig. 1. FTIR spectrum of MWCNTs-CoFe₂O₄ nanocomposite.

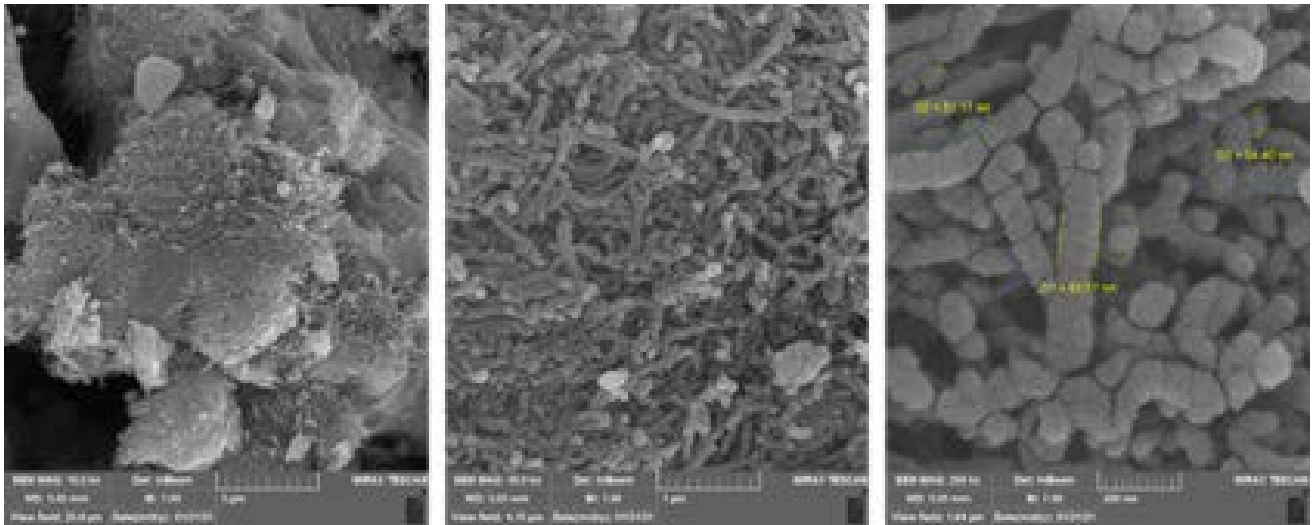


Fig. 2. FESEM images of MWCNTs-CoFe₂O₄ nanocomposite.

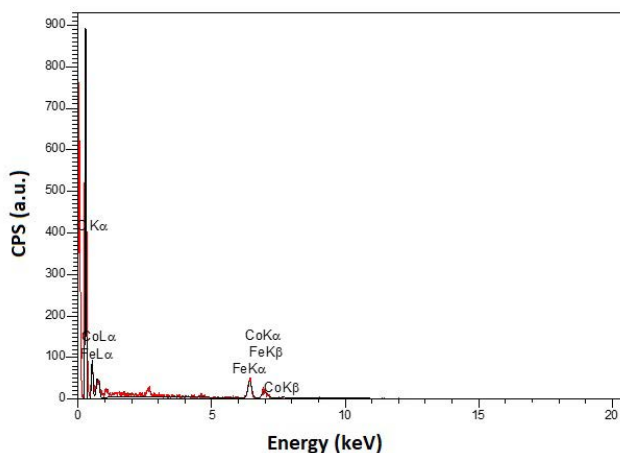


Fig. 3. Elemental analysis (EDS) of MWCNTs-CoFe₂O₄ nanocomposite.

and resolution. The result of this study is shown in Fig. 4. In this figure, the transparent filament lines represent the presence of carbon nanotubes and the dark (black) dots are the image of the available CoFe₂O₄ nanoparticles in the nanocomposite. These nanoparticles are often cubic; However, due to the accumulation of a large number of them in some places, spherical structures have been identified. As can be clearly seen in Fig. 4, CoFe₂O₄ nanoparticles are well placed on carbon nanotubes. In addition, the proper dispersion of carbon nanotubes and their greater amount than CoFe₂O₄ nanoparticles is obvious. In this regard, these images confirm the results of nanocomposite elemental analysis regarding of the constituents of its surface.

3.1.4. XRD analysis

In order to calculate the average size of the crystallite sample, XRD analysis was performed. XRD pattern of MWCNTs-CoFe₂O₄ nanocomposite is shown in Fig. 5. This

Table 2

Quantitative elemental analysis of MWCNTs-CoFe₂O₄ nanocomposites

Elt	Line	K	Kr	W%
C	Ka	0.7930	0.4539	71.34
O	Ka	0.0572	0.0328	17.39
Fe	Ka	0.1040	0.0595	7.75
Co	Ka	0.0458	0.0262	3.52
		1.0000	0.5724	100.00

analysis was performed using range from 10° to 80° radiations ($\lambda = 0.154\text{nm}$) in 2θ Cu-K α . To estimate the average size of crystals, Eq. (4), known as the Scherrer equation, was used. Accordingly, the size of the nanocomposite constituent crystals was calculated to be approximately 8 nm. The size of CoFe₂O₄ nanoparticles will increase the surface area of multi-walled carbon nanotubes.

$$d = \frac{K\lambda}{\beta \cos\theta} \quad (3)$$

where d , K , β and θ are the particle crystal size, Scherrer constant (0.94), the width at half the height of the phase peak and the diffraction angle, respectively [34].

3.1.5. Determination of specific surface area and porosity of nanocomposite by BET method

To measure the specific surface area of MWCNTs-CoFe₂O₄ nanocomposite and compare it with the specific surface area and porosity of multi-walled carbon nanotubes, BET method has been applied by nitrogen adsorption process. This method, which is based on adsorption, is a completely non-destructive method.

Also, the porosity of the synthetic nanocomposite has been measured by conventional nitrogen gas

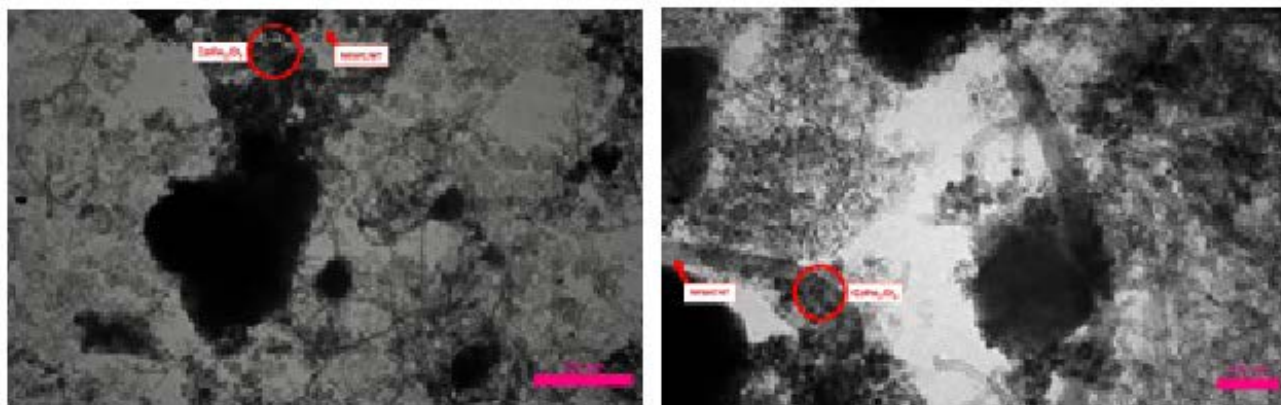


Fig. 4. TEM image of MWCNTs-CoFe₂O₄ nanocomposite.

Table 3

Comparative study of specific surface area, porosity and diameter of MWCNTs and MWCNTs-CoFe₂O₄ pores

Compounds	MWCNTs	MWCNTs-CoFe ₂ O ₄
Specific surface area (m ² /g)	73.237	113.63
Total pore volume ($p/p_0 = 0.990$) (cm ³ /g)	0.5398	0.1824
Mean pore diameter (nm)	29.48	6.4222

adsorption method under temperature of 77 K and pressure of 91.43 Kpa. In this analysis, samples of multi-walled carbon nanotubes were subjected to BET analysis, and then a comparative study was performed between changes in surface area, porosity, and pore diameter of MWCNTs and MWCNTs-CoFe₂O₄ nanocomposite. The results of this study are presented in Table 3. Based on the results, it was found that the specific surface area, porosity and also the pores diameter in MWCNTs-CoFe₂O₄ nanocomposite compared to carbon nanotubes has increased by about 35%, decreased by 66% and decreased by 78%, respectively. Since increasing the specific surface area is one of the effective points for an adsorbent, it can be said that the synthesis of this nanocomposite and its using as adsorbent has been more efficient than multi-walled carbon nanotubes. The reason for the increase in the surface area of the nanocomposite compared to multi-walled carbon nanotubes was due to the binding of CoFe₂O₄ nanoparticles to carbon nanotubes. CoFe₂O₄ nanoparticles are not a porous compound and then the porosity and pore diameter of the nanocomposite structure have been reduced compared to carbon nanotubes. This is due to the closure of cavities in the structure of carbon nanotubes due to the attachment of CoFe₂O₄ nanoparticles to their walls. These results also confirm what was said in the XRD analysis section regarding the increase in surface area of multi-walled carbon nanotubes after the binding of CoFe₂O₄ nanoparticles.

3.1.6. VSM analysis

Magnetic behavior different types of ferromagnetic, paramagnetic, and diamagnetic materials can be determined using the magnetic hysteresis curve. In order to investigate the magnetic properties of MWCNTs-CoFe₂O₄

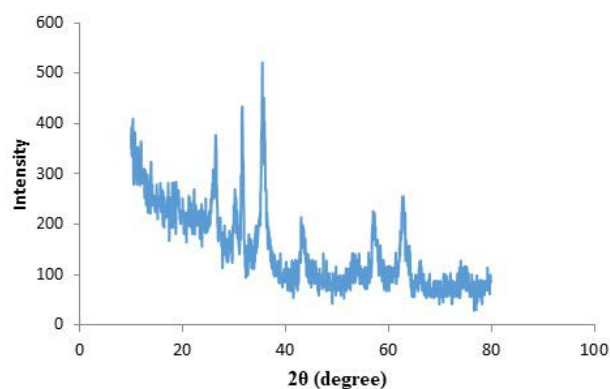


Fig. 5. XRD pattern of the MWCNTs-CoFe₂O₄ nanocomposite.

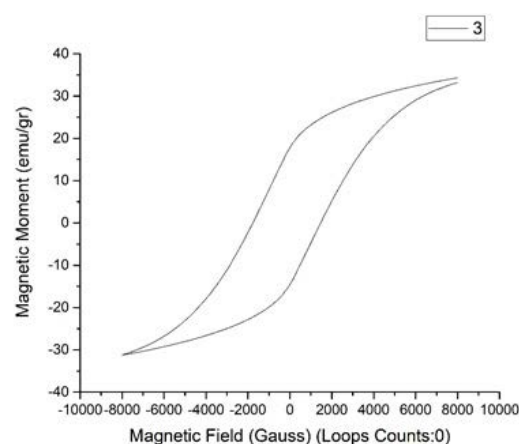


Fig. 6. Magnetization curves of MWCNTs-CoFe₂O₄.

Table 4
Parameters of isotherm models for RBBR dye adsorption on the MWCNTs-CoFe₂O₄ nanocomposite

Langmuir isotherm model			Freundlich isotherm model			Temkin isotherm model		
R ²	β	K _T	R ²	n	K _F	R ²	q _m	K _L
0.9998	7.0153	651.97	0.835	1.81	8.9866	0.7716	72.46	5.75

nanocomposite, VSM analysis was performed in the range of −10,000 to +10,000 and saturation magnetization (Ms) of −40 to +40 emu/g at room temperature. The result of this analysis is shown in Fig. 6. Based on the obtained diagram, it can be considered that the saturation magnetization of the nanocomposite is set at 34.9 emu/g. The obtained value indicates that the synthesized nanocomposite has significant magnetic properties. Based on the type of obtained curve, the ferromagnetic properties of the nanocomposite are also confirmed. Therefore, it is possible to separate this nanocomposite from the aqueous solution containing the contaminant by a magnet after the adsorption process [35,36].

3.2. Effects of factors on the removal of RBBR by MWCNTs-CoFe₂O₄ nanocomposite

3.2.1. pH effect

One of the parameters that directly affects the changes in the surface electric charge of the adsorbent and also changes in the electrostatic attraction between the adsorbate and the adsorbent is the acidity and alkalinity of the studied solution, which is expressed by the pH parameter. If the adsorbate become ionic, changes in the surface charge of the adsorbent can greatly affect the removal efficiency of the charged compound in the adsorption process. First, the pH_{pzc} point of the adsorbent was determined by the diagram shown in Fig. 7. According to this diagram, pH_{pzc} = 7.41 was obtained. This indicates that the adsorbent surface charge will be positive when the pH of the solution is less than 7.41 and negative when the pH of the solution is greater than that number. At pH = 7.41, the charge of the adsorbent surface is neutral (no charge). Then, in order to study the effect of solution pH on the removal efficiency of RBBR dye, volume of 1 L of 30 mg/L dye prepared with 298 K. HCl and NaOH were used for adjusting the pH of the solution in the range of 3–11. In this experiment, the adsorbent dose was 0.2 g/L and the contact time was 80 min. The test results are shown in Fig. 8. According to the results, it is clear that the amount of dye adsorption on the adsorbent surface has sharply decreased with increasing of solution pH. The lowest and the highest removal rate was observed in the pH = 11 and pH = 3, respectively. The reason of this observation can be discussed from two perspectives. First, the amount of OH[−] ions in solution increased in alkaline pH; As a result, competition will take place between these ions and the anionic part of the dye molecule in solution for the occupation of active adsorbent sites. Since size of OH[−] ions is smaller than the volume of the anionic part of the dye molecule, this ion will win the competition and will occupy the active sites of the adsorbent [37]. Second, in alkaline

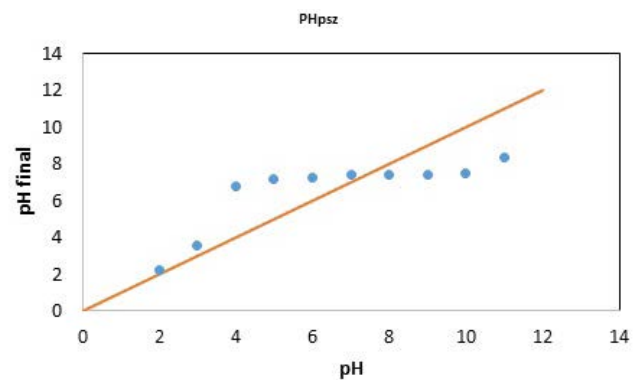


Fig. 7. Determination of pH_{pzc} of MWCNTs-CoFe₂O₄ nanocomposite.

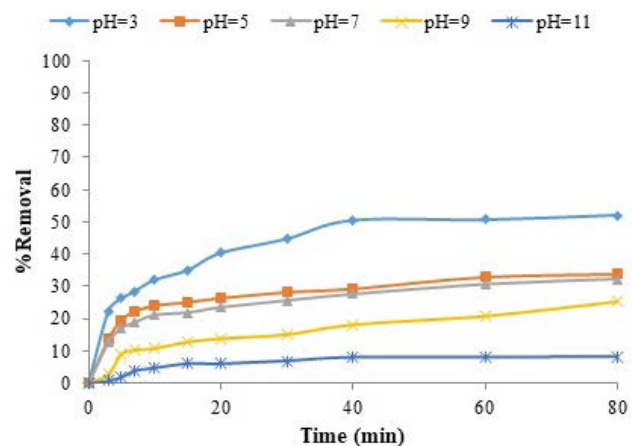


Fig. 8. Effect of pH changes on removal efficiency of RBBR dye.

pH and the placement of OH[−] ions on the adsorbent surface, the surface will be negative, and as a result, due to the electrostatic repulsion that will occur between the OH[−] ions and the anionic part of the dye molecule, the amount of dye adsorption on active surfaces will decrease. For this reason, the removal efficiency of the dye molecule has significantly decreased with increasing the pH of the solution. With decreasing alkalinity of the solution, the removal efficiency increased and reached to its maximum value (approximately 94%) in the acidic pH (pH = 3). In acidic media, the H⁺ ions in solution increase and cover the adsorbent surface in a similar way. With the emergence of electrostatic attraction between the surface of the adsorbent coated with H⁺ ions and the anionic dye, the removal efficiency has increased. Accordingly, pH = 3 was selected as the optimal pH and used in the next experiments.

3.2.2. Effect of nanocomposite dosage

Determining the optimal amount of adsorbent as one of the main parameters in the adsorption process is important. Requiring the optimal dosage of adsorbent is significant from two aspects. From the first aspect, the goal of the optimal use of adsorbent is increasing the removal efficiency of pollutant and from the second aspect; it is to prevent excessive use of the adsorbent after optimizing its amount. As a result, it is economically viable. For this purpose, dyes solutions in 1 L volume and initial concentration of 30 mg/L were prepared from the stoke solution and effect of the nanocomposite dosage on the removal efficiency was studied in the range of 0.1–1 g/L in the experimental conditions of temperature = 298 K, contact time = 80 min and pH = 3. The results of this study are shown in Fig. 9. Based on the results, it was found that increasing the adsorbent dose from 0.1 to 0.4 g/L increased removal efficiency of organic dye. The reason for this is that when the adsorbent dose increases, active sites become available in the adsorption process. This mechanism will have a direct effect on increasing the removal efficiency. But with increasing the adsorbent dose from 0.4 to 1 g/L, it is observed that the removal efficiency has decreased step by step. The cause of this phenomenon can be due to agglomeration of nanoparticles in the solution as a result of excessive use of adsorbent. Agglomeration can reduce the active sites of the adsorbent, and ultimately reduces the efficiency of dye removal [38]. In addition, according to the graph shown in Fig. 10, it is observed that in the initial times of the process (first 10 min), the rate of removal process is very high due to available sites of adsorbent, but with increasing the time from 10 to 80 min, this trend has decreased significantly. The reason for this is that over time and due to the occupation of active sites by pollutants, these sites has declined, resulting in the decreased removal efficiency. Based on the results, the optimal dosage of MWCNTs-CoFe₂O₄ Nano composite for RBBR dye removal was selected 0.4 g/L. Also, based on the results in two recent experiments, the optimal time for the organic dye removal by the MWCNTs-CoFe₂O₄ nanocomposite was obtained 40 min. Because there is no significant, change in the organic dye removal efficiency in more than 40 min.

3.2.3. Effect of initial concentration of RBBR dye

Another effective parameter on the pollutant removal efficiency in the adsorption process is the initial concentration of pollutant in the solution. In order to study the effect of this parameter on the removal efficiency and also to obtain the necessary experimental information for studying the process kinetics and determination the type of removal process mechanism by matching the experimental data with different isothermal equations, dye solutions in a volume of 1 L and different concentrations 10, 20, 50, 100 and 200 mg/L were prepared and experiments were performed under the experimental conditions of pH = 3, dosage 0.4 g/L and temperature of 298 K. The results of this study are shown in Fig. 10. The experimental results clearly show that the contaminant removal efficiency has decreased with increasing the initial concentration of dye. The cause of this

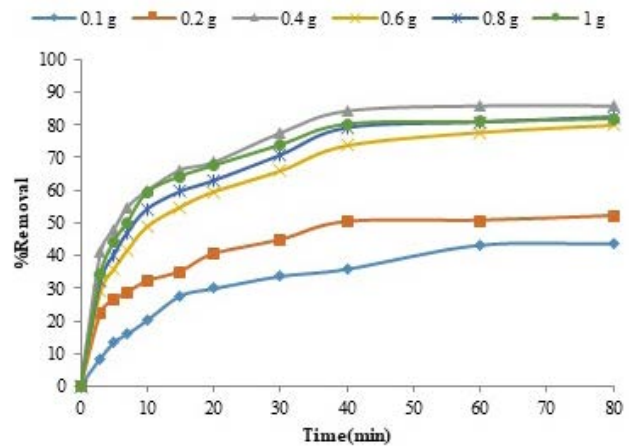


Fig. 9. Effect of adsorbent dosage changes on RBBR dye removal efficiency.

phenomenon can be attributed to the decrease of adsorbent capacity for dye adsorption with increasing the dye concentration. Therefore, it is obvious that removal efficiency has decreased with increasing the dye concentration. Therefore, a concentration of 20 mg/L was selected as the optimal concentration of the process [39–41].

3.2.4. Effect of temperature

In this study, the effect of temperature parameter on dye removal efficiency was also investigated in order to study and calculate the thermodynamic parameters of the process. For this purpose, 1 L of dye with 20 mg/L concentration prepared in pH = 3 and 0.4 g of adsorbent was added to them. This study was performed at three temperatures of 308, 318 and 328 K, and the results of this study are shown in Fig. 11. Based on these results, it can be said that temperature changes did not have a significant effect on the process efficiency. However, looking at the general trend of changes, it was observed that slight increase in temperature has reduced the removal efficiency of organic dyes [42].

3.3. Study of isotherms

The experimental data obtained in this research were matched with three different models of isotherms including Langmuir, Freundlich and Temkin isotherms. Eqs. (4)–(6) are related to the Langmuir, Freundlich and Temkin isotherms, respectively.

$$\frac{C_e}{q_e} = \frac{1}{q_m} (C_e) + \frac{1}{K_L q_m} \tag{4}$$

$$\text{Log } q_e = \text{Log } K_F + \frac{1}{n} \text{Log } C_e \tag{5}$$

$$q_e = \beta \ln K_T + \beta \ln C_e \tag{6}$$

where C_e , q_e , q_m , K_L , K_F and β are equilibrium concentration (mg/L), equilibrium capacity, maximum capacity (mg/g),

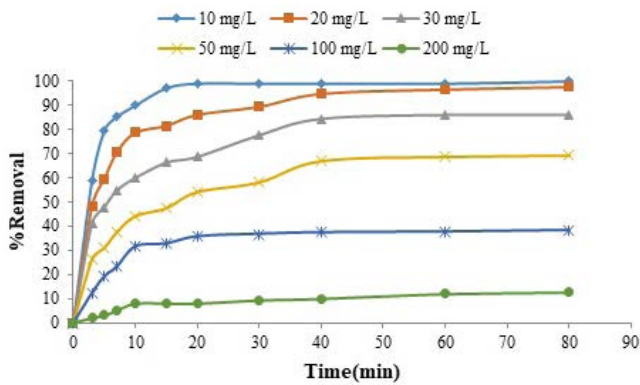


Fig. 10. Effect of initial concentration changes on RBBR dye removal efficiency.

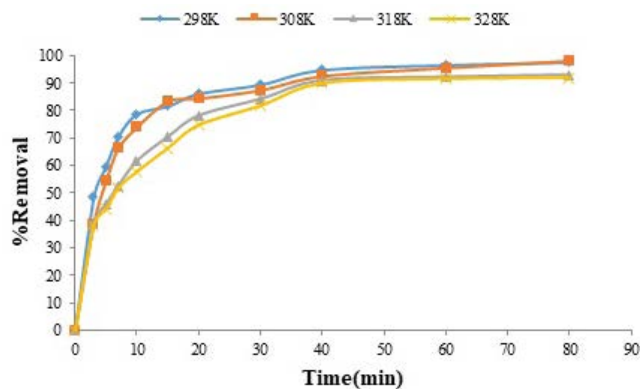


Fig. 11. Effect of temperature changes on RBBR dye removal efficiency.

Langmuir constant (L/mg), Freundlich (mg/g/(mg/L)^{1/n}), Temkin constant (L/mg) and the parameter related to the maximum connection energy (J/mol), respectively [42–45]. The results of this study are shown in Fig. 12 and the regression coefficient and the constants related to each of these isotherms are shown in Table 4. Based on the results, it has been determined that the experimental data obtained from the removal of RBBR dye by MWCNTs-CoFe₂O₄ nanocomposite based-adsorbent have shown high compatibility with Langmuir isotherm. Accordingly, it can be said that the surface of the synthetic nanocomposite is homogeneous and the dye adsorption on the adsorbent surface has occurred in a single layer [40,42].

3.4. Kinetic study

To investigate the dynamics and the factors affecting the rate of RBBR dye adsorption process, kinetic study of the process is necessary. The obtained experimental data were matched with two kinetic models of pseudo-first-order equation [Eq. (7)] and pseudo-second-order [Eq. (8)]:

$$\ln(q_e - q_t) = -k_1 t + \ln q_e \tag{7}$$

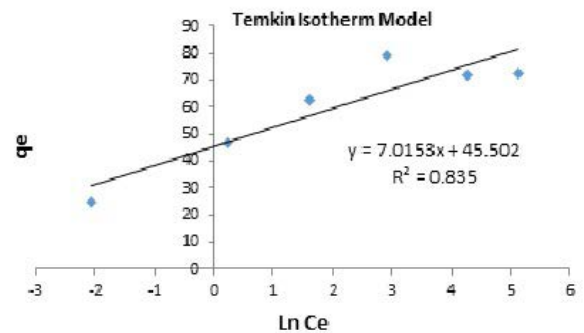
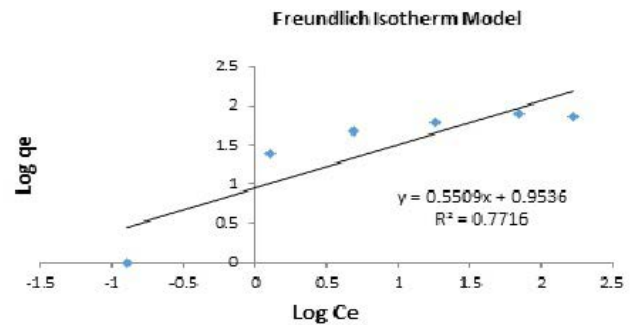
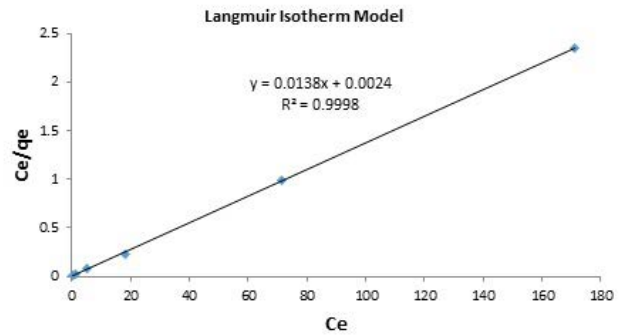


Fig. 12. Langmuir, Freundlich and Temkin isotherms.

$$\frac{1}{q_e k_2} \frac{t}{q_t} = \frac{1}{q_e} + t \tag{8}$$

where t , q_t , K_1 and K_2 are time (min), capacity at time t (mg/g), rate constants related to the pseudo-first-order kinetic model (min⁻¹) and pseudo-second-order (g/mg min), respectively [46–49]. The results of this study are shown in Fig. 13 and Table 5. The results of the calculations indicate that the data are well matched to the pseudo-second-order kinetic equation. It is found that the occupancy rate of active sites of adsorbent is proportional to the square of empty sites. Therefore, it can be said that according to the obtained regression coefficient and the agreement of the data with the pseudo-second-order model, these indicate that chemisorption is relatively dominant and controls the adsorption process for RBBR dye adsorption using MWCNTs-CoFe₂O₄ nanocomposite [50,51]. In Table 6,

the maximum adsorption capacity (q_{\max}) of several similar adsorbents in different studies has been shown; the q_{\max} of the MWCNTs-CoFe₂O₄ nanocomposite was 106.5 mg/g, which is considered to be efficient compared to other similar adsorbents and nanocomposite (Table 6).

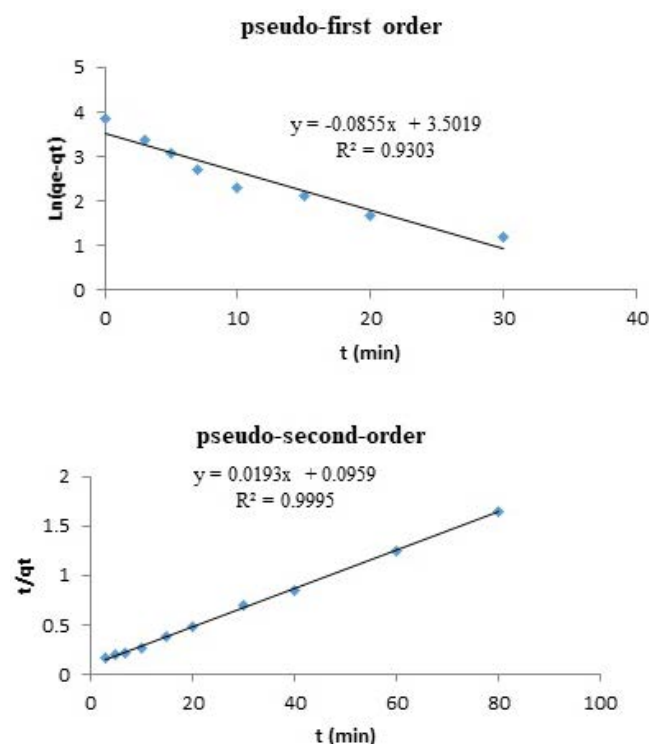


Fig. 13. Kinetic models of RBBR dye adsorption process in the presence of MWCNTs-CoFe₂O₄ nanocomposite.

Table 5
Kinetic models coefficients for RBBR dye adsorption in the presence of MWCNTs-CoFe₂O₄ nanocomposite

Pseudo-first-order model			Pseudo-second-order model		
q_e	K_2	R^2	q_e	K_1	R^2
51.81	0.0038	0.9995	33.17	0.0855	0.9303

Table 6
Comparison of the adsorption for RBBR dye adsorption in the presence of MWCNTs-CoFe₂O₄ nanocomposite and other reported adsorbents

Adsorbent	q_{\max} (mg/g)	Reference
MWCNTs-CoFe ₂ O ₄ nanocomposite	106.5	This study
Agro-industrial waste <i>Jatropha curcas</i> pods as an activated carbon	237.5	[55]
Sewage activated carbon	33.5	[56]
Peanut hull-based H ₃ PO ₄ activated carbon	149.2	[57]
Magnetic chitosan-glutaraldehyde/zinc oxide/Fe ₃ O ₄ nanocomposite	176.6	[58]
Ultraporous aluminas (UPA)	122.5	[59]
<i>Aspergillus tubingensis</i>	143	[60]
Poly[2-hydroxy-3-(1-naphthylxy)propyl] methacrylate [poly(NOPMA)]	60.8	[61]

3.5. Thermodynamic study

Based on the data obtained from experiments related to the effect of temperature changes on removal efficiency of RBBR dye, thermodynamic parameters of the process including Gibbs free energy changes (ΔG), enthalpy changes (ΔH) and entropy changes (ΔS) can be calculated from Eqs. (9) and (10) [52,53].

$$\Delta G_{ad}^0 = -RT \ln K(T) K(T) = \frac{q_e}{C_e} \quad (9)$$

$$\ln K(T) = -\frac{\Delta H_{ad}^0}{R} \left(\frac{1}{T} \right) + \frac{\Delta S_{ad}^0}{R} \quad (10)$$

The results of this study are shown in Fig. 14 and Table 7. According to the results, it is clear that this process is exothermic and spontaneous. The standard free energy (ΔG°) was negative at different temperatures, indicating spontaneity and applicability of the process. The negative value of ΔH° (-32.38 kJ/mol) indicates that the adsorption process has small adsorption heat and is exothermic. The increase of temperature will facilitate the activity of molecule and disturb the stable adsorb, consequently restricts the adsorption capacity [54]. That is consistent with the results of adsorption capacity at different temperatures.

4. Conclusion

In this research, MWCNTs-CoFe₂O₄ nanocomposite synthesized, characterized and used as an effective magnetic adsorbent for removal of RBBR organic dye. The optimal values of each of the parameters were determined as 40 min, 0.4 g, 20 mg/L, 3 and 298 K, respectively. Based on the isotherm models analysis, the adsorption data were found to be best described by the Langmuir isotherm model. The kinetic study also showed that the process follows a pseudo-second-order kinetic model. The maximum adsorption capacity (q_{\max}) of MWCNTs-CoFe₂O₄ for RBBR dye was 106.5 mg/g. Based on the thermodynamic studies, it was found that the adsorption process is exothermic and spontaneous and associated with a decrease in entropy. Therefore, considering these conditions, MWCNTs-CoFe₂O₄ nanocomposite can be used to remove antibiotic contaminants from water sources.

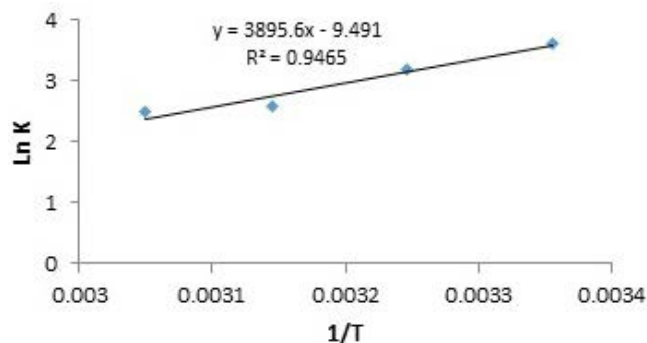


Fig. 14. Thermodynamic study for adsorption process of RBBR dye by MWCNTs-CoFe₂O₄ nanocomposite based-adsorbent.

Table 7

Thermodynamic parameters of RBBR dye adsorption by MWCNTs-CoFe₂O₄ nanocomposite

Temperature (K)	ΔG (kJ/mol)	ΔH (kJ/mol)	ΔS (kJ/mol K)
298	-8.93	-32.38	-0.078
308	-8.2		
318	-6.82		
328	-6.79		

Acknowledgment

This paper was a part of faculty approved research project and supported financially by a grant (No: IR.GUMS.REC.1399.394) from the Guilan University of Medical Sciences, Rasht, Iran. The authors need to thank the University for its Support.

References

- [1] A. Karami, K. Karimyan, R. Davoodi, M. Karimaei, K. Sharafie, S. Rahimi, T. Khosravi, M. Miri, H. Sharafi, A. Azari, Application of response surface methodology for statistical analysis, modeling, and optimization of malachite green removal from aqueous solutions by manganese-modified pumice adsorbent, *Desal. Water Treat.*, 89 (2017) 150–161.
- [2] S.S. Behera, D. Sourav, P.K. Parhi, S.K. Tripathy, R.K. Mohapatra, D. Mayadhar, Kinetics, thermodynamics and isotherm studies on adsorption of methyl orange from aqueous solution using ion exchange resin Amberlite IRA-400, *Desal. Water Treat.*, 60 (2017) 249–260.
- [3] A. Azari, R. Nabizadeh, S. Nasser, A.H. Mahvi, A.R. Mesdaghinia, Comprehensive systematic review and meta-analysis of dyes adsorption by carbon-based adsorbent materials: classification and analysis of last decade studies, *Chemosphere*, 250 (2020) 126238, doi: 10.1016/j.chemosphere.2020.126238.
- [4] S.Z. Ghazanfari, J. Jaafari, S.D. Ashrafi, K. Taghavi, Decolourisation of direct red dye 81 from aqueous solutions by SnO₂/H₂O₂ hybrid process, *Int. J. Environ. Anal. Chem.*, (2021) 1–15, doi: 10.1080/03067319.2021.1921758.
- [5] J. Jaafari, H. Barzanouni, S. Mazloomi, N.A.A. Farahani, K. Sharafi, P. Soleimani, G.A. Haghighat, Effective adsorptive removal of reactive dyes by magnetic chitosan nanoparticles: kinetic, isothermal studies and response surface methodology, *Int. J. Biol. Macromol.*, 164 (2020) 344–355.
- [6] A. Kausar, M. Iqbal, A. Javed, K. Aftab, H.N. Bhatti, S. Nouren, Dyes adsorption using clay and modified clay: a review, *J. Mol. Liq.*, 256 (2018) 395–407.
- [7] D. Naghipour, L. Hoseinzadeh, K. Taghavi, J. Jaafari, A. Amouei, Effective removal of tetracycline from aqueous solution using biochar prepared from pine bark: isotherms, kinetics and thermodynamic analyses, *Int. J. Environ. Anal. Chem.*, (2021) 1–14, doi: 10.1080/03067319.2021.1942462.
- [8] S. Yavari, N.M. Mahmodi, P. Teymouri, B. Shahmoradi, A. Maleki, Cobalt ferrite nanoparticles: preparation, characterization and anionic dye removal capability, *J. Taiwan Inst. Chem. Eng.*, 59 (2016) 320–329.
- [9] D. Naghipour, J. Jaafari, S.D. Ashrafi, A.H. Mahvi, Remediation of heavy metals contaminated silty clay loam soil by column extraction with ethylenediaminetetraacetic acid and nitrilo triacetic acid, *J. Environ. Eng.*, 143 (2017) 04017026, doi: 10.1061/(ASCE)EE.1943-7870.0001219.
- [10] M. Esmailzadeh, J. Jaafari, A.A. Mohammadi, M. Panahandeh, A. Javid, S. Javan, Investigation of the extent of contamination of heavy metals in agricultural soil using statistical analyses and contamination indices, *Hum. Ecol. Risk Assess.*, 25 (2019) 1125–1136.
- [11] D. Naghipour, L. Hoseinzadeh, K. Taghavi, J. Jaafari, Characterization, kinetic, thermodynamic and isotherm data for diclofenac removal from aqueous solution by activated carbon derived from pine tree, *Data Brief*, 18 (2018) 1082–1087.
- [12] J. Cheng, C. Zhan, J. Wu, Z. Cui, J. Si, Q. Wang, X. Peng, L.-S. Turng, Highly efficient removal of methylene blue dye from an aqueous solution using cellulose acetate nanofibrous membranes modified by polydopamine, *ACS Omega*, 5 (2020) 5389–5400.
- [13] S. Wong, N. Abd Ghafar, N. Ngadi, F.A. Razmi, I.M. Inuwa, R. Mat, N.A.S. Amin, Effective removal of anionic textile dyes using adsorbent synthesized from coffee waste, *Sci. Rep.*, 10 (2020) 1–13.
- [14] M.T. Yagub, T.K. Sen, S. Afroz, H.M. Ang, Dye and its removal from aqueous solution by adsorption: a review, *Adv. Colloid Interface Sci.*, 209 (2014) 172–184.
- [15] S. Banerjee, M. Chattopadhyaya, Adsorption characteristics for the removal of a toxic dye, tartrazine from aqueous solutions by a low cost agricultural by-product, *Arabian J. Chem.*, 10 (2017) S1629–S1638.
- [16] F. Hosseini, S. Sadighian, H. Hosseini-Monfared, N.M. Mahmoodi, Dye removal and kinetics of adsorption by magnetic chitosan nanoparticles, *Desal. Water Treat.*, 57 (2016) 24378–24386.
- [17] A.R. Abhari, A.A. Safekordi, M.E. Olya, N.M. Mahmoodi, Synthesis of PVDF nanocomposite surface-modified membrane containing ZnO: Ca for dye removal from colored wastewaters in a fixed-bed photocatalytic-membrane reactor, *Desal. Water Treat.*, 138 (2019) 36–48.
- [18] A. Sharifi, L. Montazerghaem, A. Naeimi, A.R. Abhari, M. Vafaei, G.A. Ali, H. Sadegh, Investigation of photocatalytic behavior of modified ZnS: Mn/MWCNTs nanocomposite for organic pollutants effective photodegradation, *J. Environ. Manage.*, 247 (2019) 624–632.
- [19] D.J. Naghan, A. Azari, N. Mirzaei, A. Velayati, F.A. Tapouk, S. Adabi, M. Pirsaeheb, K. Sharafi, Parameters effecting on photocatalytic degradation of the phenol from aqueous solutions in the presence of ZnO nanocatalyst under irradiation of UV-C light, *Bulg. Chem. Commun.*, 47 (2015) 14–18.
- [20] S. Umoren, U. Etim, A. Israel, Adsorption of methylene blue from industrial effluent using poly(vinyl alcohol), *J. Mater. Environ. Sci.*, 4 (2013) 75–86.
- [21] Y. Wan, Z.-Y. Liu, P. Song, X.-Q. Zhang, J.-C. Song, Y.-J. Fu, X.-H. Yao, J. Wang, T. Chen, D.-Y. Zhang, Ionic liquid groups modified 3D porous cellulose microspheres for selective adsorption of AO7 dye, *J. Cleaner Prod.*, 240 (2019) 118201, doi: 10.1016/j.jclepro.2019.118201.
- [22] R. Li, J. Liu, A. Shi, X. Luo, J. Lin, R. Zheng, H. Fan, S.V. Selasie, H. Lin, A facile method to modify polypropylene membrane by polydopamine coating via inkjet printing technique for superior performance, *J. Colloid Interface Sci.*, 552 (2019) 719–727.
- [23] A. Khojastehnezhad, F. Moieinpour, A. Javid, NiFe₂O₄@SiO₂-PPA nanoparticle: a green nanocatalyst for the synthesis of

- β-acetamido ketones, *Polycyclic Aromat. Compd.*, 39 (2019) 404–412.
- [24] M. Rahimizadeh, S.M. Seyedi, M. Abbasi, H. Eshghi, A. Khojastehnezhad, F. Moeinpour, M. Bakavoli, Nanomagnetically modified ferric hydrogen sulfate ($\text{NiFe}_2\text{O}_4/\text{SiO}_2\text{-FHS}$): a reusable green catalyst for the synthesis of highly functionalized piperidine derivatives, *J. Iran. Chem. Soc.*, 12 (2015) 839–844.
- [25] A. Azari, M. Salari, M.H. Dehghani, M. Alimohammadi, H. Ghaffari, K. Sharafi, N. Shariatifar, M. Baziar, Efficiency of magnitized graphene oxide nanoparticles in removal of 2,4-dichlorophenol from aqueous solution, *J. Mazandaran Univ. Med. Sci.*, 26 (2017) 265–281.
- [26] P. Beigzadeh, F. Moeinpour, Fast and efficient removal of silver(I) from aqueous solutions using *Aloe vera* shell ash supported $\text{Ni}_{0.5}\text{Zn}_{0.5}\text{Fe}_2\text{O}_4$ magnetic nanoparticles, *Trans. Nonferrous Met. Soc. China*, 26 (2016) 2238–2246.
- [27] M. Rouhani, S.D. Ashrafi, K. Taghavi, M.N. Joubani, J. Jaafari, Evaluation of tetracycline removal by adsorption method using magnetic iron oxide nanoparticles (Fe_3O_4) and clinoptilolite from aqueous solutions, *J. Mol. Liq.*, 356 (2022) 119040, doi: 10.1016/j.molliq.2022.119040.
- [28] X. Li, C. Sun, W. Cao, C. Hu, Y. Zhao, Comparative adsorption of remazol brilliant blue R and copper in aqueous solutions by carbon nanotubes with different levels of carboxyl group and specific surface area, *Mater. Res. Express.*, 6 (2019) 1050e2.
- [29] M.C. Arya, P.S. Bafila, D. Mishra, K. Negi, R. Kumar, A. Bughani, Adsorptive removal of Remazol Brilliant Blue R dye from its aqueous solution by activated charcoal of *Thuja orientalis* leaves: an eco-friendly approach, *SN Appl. Sci.*, 2 (2020) 1–10.
- [30] L.U. Khan, M. Younas, S.U. Khan, M.Z.U. Rehman, Synthesis and characterization of $\text{CoFe}_2\text{O}_4/\text{MWCNTs}$ nanocomposites and high-frequency analysis of their dielectric properties, *J. Mater. Eng. Perform.*, 29 (2020) 251–258.
- [31] B. Unal, M. Senel, A. Baykal, H. Sözeri, Multiwall-carbon nanotube/cobalt ferrite hybrid: synthesis, magnetic and conductivity characterization, *Curr. Appl. Phys.*, 13 (2013) 1404–1412.
- [32] M. Goodarz Naseri, E.B. Saion, A. Kamali, An overview on nanocrystalline ZnFe_2O_4 , MnFe_2O_4 , and CoFe_2O_4 synthesized by a thermal treatment method, *Int. Sch. Res. Notices*, 2012 (2012) 604241, doi: 10.5402/2012/604241.
- [33] G. Allaadini, S.M. Tasirin, P. Aminayi, Magnetic properties of cobalt ferrite synthesized by hydrothermal method, *Int. Nano Lett.*, 5 (2015) 183–186.
- [34] M. Margabandhu, S. Sendhilkumar, S. Senthilkumar, D. Gajalakshmi, Investigation of structural, morphological, magnetic properties and biomedical applications of Cu^{2+} substituted uncoated cobalt ferrite nanoparticles, *Braz. Arch. Biol. Technol.*, 59 (2017) 1–10.
- [35] S. Das, C. Manoharan, M. Venkateshwarlu, P. Dhamodharan, Structural, optical, morphological and magnetic properties of nickel doped cobalt ferrite nanoparticles synthesized by hydrothermal method, *J. Mater. Sci.: Mater. Electron.*, 30 (2019) 19880–19893.
- [36] R. Tabit, O. Amadine, Y. Essamlali, K. Dânoun, A. Rhihil, M. Zahouily, Magnetic CoFe_2O_4 nanoparticles supported on graphene oxide ($\text{CoFe}_2\text{O}_4/\text{GO}$) with high catalytic activity for peroxymonosulfate activation and degradation of rhodamine B, *RSC Adv.*, 8 (2018) 1351–1360.
- [37] C.M. Simonescu, A. Tătăruș, D.C. Culiță, N. Stănică, I.A. Ionescu, B. Butoi, A.-M. Banici, Comparative study of CoFe_2O_4 nanoparticles and CoFe_2O_4 -chitosan composite for Congo red and Methyl orange removal by adsorption, *Nanomaterials (Basel)*, 11 (2021) 711, doi: 10.3390/nano11030711.
- [38] A.A. Farghali, M. Bahgat, W.M. ElRouby, M.H. Khedr, Decoration of multi-walled carbon nanotubes (MWCNTs) with different ferrite nanoparticles and its use as an adsorbent, *J. Nanostruct. Chem.*, 3 (2013) 1–12.
- [39] A. Farghali, M. Bahgat, W. El Roubay, M. Khedr, Decoration of MWCNTs with CoFe_2O_4 nanoparticles for methylene blue dye adsorption, *J. Solution Chem.*, 41 (2012) 2209–2225.
- [40] N.M. Mahmoodi, O. Masrouri, Cationic dye removal ability from multicomponent system by magnetic carbon nanotubes, *J. Solution Chem.*, 44 (2015) 1568–1583.
- [41] E. Girgis, D. Adel, C. Tharwat, O. Attallah, K.V. Rao, Cobalt ferrite nanotubes and porous nanorods for dye removal, *Adv. Nano Res.*, 3 (2015) 111–121.
- [42] O.A. Oyetade, V.O. Nyamori, B.S. Martincigh, S.B. Jonnalagadda, Effectiveness of carbon nanotube–cobalt ferrite nanocomposites for the adsorption of rhodamine B from aqueous solutions, *RSC Adv.*, 5 (2015) 22724–22739.
- [43] M.D. Yahya, K.S. Obayomi, M.B. Abdulkadir, Y.A. Iyaka, A.G. Olugbenga, Characterization of cobalt ferrite-supported activated carbon for removal of chromium and lead ions from tannery wastewater via adsorption equilibrium, *Water Sci. Eng.*, 13 (2020) 202–213.
- [44] L. Ai, M. Li, L. Li, Adsorption of methylene blue from aqueous solution with activated carbon/cobalt ferrite/alginate composite beads: kinetics, isotherms, and thermodynamics, *J. Chem. Eng. Data*, 56 (2011) 3475–3483.
- [45] M. Rajabi, K. Mahanpoor, O. Moradi, Removal of dye molecules from aqueous solution by carbon nanotubes and carbon nanotube functional groups: critical review, *RSC Adv.*, 7 (2017) 47083–47090.
- [46] K. Vamvakidis, T.-M. Kostitsi, A. Makridis, C. Dendrinou-Samara, Diverse surface chemistry of cobalt ferrite nanoparticles to optimize copper(II) removal from aqueous media, *Materials (Basel)*, 13 (2020) 1537, doi: 10.3390/ma13071537.
- [47] A.A. Badawy, S.M. Ibrahim, H.A. Essawy, Enhancing the textile dye removal from aqueous solution using cobalt ferrite nanoparticles prepared in presence of fulvic acid, *J. Inorg. Organomet. Polym. Mater.*, 30 (2020) 1798–1813.
- [48] D.P. Dutta, R. Venugopalan, S. Chopade, Manipulating carbon nanotubes for efficient removal of both cationic and anionic dyes from wastewater, *ChemistrySelect*, 2 (2017) 3878–3888.
- [49] D. Naghipour, K. Taghavi, J. Jaafari, I. Kabdaşlı, M. Makkiabadi, M. Javan Mahjoub Doust, F. Javan Mahjoub Doust, Scallop shell coated Fe_3O_4 nanocomposite as an eco-friendly adsorbent for tetracycline removal, *Environ. Technol.*, (2021) 1–11, doi: 10.1080/09593330.2021.1966105.
- [50] D. Naghipour, K. Taghavi, M. Ashournia, J. Jaafari, R. Arjmand Movarrehk, A study of Cr(VI) and NH_4^+ adsorption using greensand (glaucanite) as a low-cost adsorbent from aqueous solutions, *Water Environ. J.*, 34 (2020) 45–56.
- [51] S.D. Ashrafi, G.H. Safari, K. Sharafi, H. Kamani, J. Jaafari, Adsorption of 4-nitrophenol on calcium alginate-multiwall carbon nanotube beads: modeling, kinetics, equilibria and reusability studies, *Int. J. Biol. Macromol.*, 185 (2021) 66–76.
- [52] S. Ahmadi, L. Mohammadi, A. Rahdar, S. Rahdar, R. Dehghani, C. Adaobi Igwegbe, G.Z. Kyzas, Acid dye removal from aqueous solution by using neodymium(III) oxide nano-adsorbents, *Nanomaterials (Basel)*, 10 (2020) 556, doi: 10.3390/nano10030556.
- [53] N.N. Rudi, M.S. Muhamad, L. Te Chuan, J. Alipal, S. Omar, N. Hamidon, N.H.A. Hamid, N.M. Sunar, R. Ali, H. Harun, Evolution of adsorption process for manganese removal in water via agricultural waste adsorbents, *Heliyon*, 6 (2020) e05049, doi: 10.1016/j.heliyon.2020.e05049.
- [54] Q. Song, Y. Fang, Z. Liu, L. Li, Y. Wang, J. Liang, Y. Huang, J. Lin, L. Hu, J. Zhang, The performance of porous hexagonal BN in high adsorption capacity towards antibiotics pollutants from aqueous solution, *Chem. Eng. J.*, 325 (2017) 71–79.
- [55] P. Sathishkumar, M. Arulkumar, T. Palvannan, Utilization of agro-industrial waste *Jatropha curcas* pods as an activated carbon for the adsorption of reactive dye Remazol Brilliant Blue R (RBBR), *J. Cleaner Prod.*, 22 (2012) 67–75.
- [56] T.L. Silva, A. Ronix, O. Pezoti, L.S. Souza, P.K. Leandro, K.C. Bedin, K.K. Beltrame, A.L. Cazetta, V.C. Almeida, Mesoporous activated carbon from industrial laundry sewage sludge: adsorption studies of reactive dye Remazol Brilliant Blue R, *Chem. Eng. J.*, 303 (2016) 467–476.
- [57] Z.-Y. Zhong, Q. Yang, X.-M. Li, K. Luo, Y. Liu, G.-M. Zeng, Preparation of peanut hull-based activated carbon by microwave-induced phosphoric acid activation and its

- application in Remazol Brilliant Blue R adsorption, *Ind. Crops Prod.*, 37 (2012) 178–185.
- [58] A. Reghioua, D. Barkat, A.H. Jawad, A.S. Abdulhameed, S. Rangabhashiyam, M.R. Khan, Z.A. AlOthman, Magnetic chitosan-glutaraldehyde/zinc oxide/Fe₃O₄ nanocomposite: optimization and adsorptive mechanism of remazol brilliant blue R dye removal, *J. Polym. Environ.*, 29 (2021) 3932–3947.
- [59] H. Xu, G. Boeuf, Z. Jia, K. Zhu, M. Nikravech, A. Kanaev, R. Azouani, M. Traore, A. Elm'selmi, Solvent-free synthesized monolithic *Ultraporous aluminas* for highly efficient removal of Remazol Brilliant Blue R: equilibrium, kinetic, and thermodynamic studies, *Materials*, 14 (2021) 3054, doi: 10.3390/ma14113054.
- [60] S.E. Karatay, Z. Aksu, İ. Özeren, G. Dönmez, Potentiality of newly isolated *Aspergillus tubingensis* in biosorption of textile dyes: equilibrium and kinetic modeling, *Biomass Convers. Biorefin.*, (2021) 1–8, doi: 10.1007/s13399-021-01523-9.
- [61] G. Torgut, M. Tanyol, F. Biryani, G. Pihtili, K. Demirelli, Application of response surface methodology for optimization of Remazol Brilliant Blue R removal onto a novel polymeric adsorbent, *J. Taiwan Inst. Chem. Eng.*, 80 (2017) 406–414.